AIAA JOURNAL
Vol. 48, No. 11, November 2010

Broadband Noise Due to Rotor-Wake/Rotor Interaction in Contra-Rotating Open Rotors

Vincent P. Blandeau* and Phillip F. Joseph†
University of Southampton, Southampton, England SO17 1BJ, United Kingdom

DOI: 10.2514/1.J050566

A semi-analytical model for the prediction of the broadband noise due to the interaction between turbulent rotor wakes and a rotor in contra-rotating open rotors is presented. The unsteady loading of the rear rotor is modeled using classical isolated flat-plate theory. Strip theory is used to treat the spanwise variations of aerodynamic quantities and blade geometry. The turbulent wake is assumed to be homogeneous and isotropic turbulence that is modulated by a train of wake profiles. The model is presented in detail and insight into its modal behavior is provided. A parameter study is conducted to investigate the effects of blade number, rotor–rotor gap and rotor speeds on broadband noise emissions due to rotor–wake/rotor interaction in contra-rotating open rotors. Scaling laws for sound power levels have been established analytically and show good agreement with the results of the parameter study.

Nomenclature

a	=	empirical wake parameter
B_i	=	blade number of the ith rotor
b_W	=	half-wake width, m
C_d	=	drag coefficient of front airfoils
c_0	=	speed of sound, m.s^{-1}
c_i	=	blade chord, m
c_l	=	azimuthal phase speed of the mode l, m.s^{-1}
$d\mathbf{F}$	=	point force per unit area applied by a blade element to the fluid, kg.m^{-1}.s^{-2}
d_i	=	azimuthal gap between blades, m
f_m	=	Fourier components of wake profile
f_W	=	wake profile function
f_{ref}	=	baseline frequency for spectrum normalization, $f_{\text{ref}} = B_2\Omega_2/2\pi$, Hz
g	=	flat-plate response function
$K_{X,qmn}$, $K_{Y,qmn}$	=	discrete values taken by k_X and k_Y, m^{-1}
$\mathbf{k} = (k_r, k_X, k_Y)$	=	turbulent wavenumber vector in spanwise, chordwise and normal directions, m^{-1}
k_0	=	acoustic wavenumber, m^{-1}
L	=	turbulence integral lengthscale, m
L_{qmn}	=	aerodynamic-acoustic coupling integral along the chord of the airfoils
l	=	azimuthal acoustic interaction mode order
$l_{\max}$	=	limit above which the modes l are cut off
M_W	=	Mach number of the mean gust velocity
M_x	=	axial flight Mach number
$M_{\phi i}$	=	rotation Mach number of a blade section of the ith rotor
m, n	=	scattering indices for front and rear rotors, respectively
$m_{\max}$	=	limit for summation over m
N_j	=	number of strips
q	=	turbulence azimuthal mode order
R_0	=	source to observer distance, m
$\bar{r}_j$	=	spanwise location of the midpoint of the jth strip, m
S_2	=	total surface area of rear rotor blades, m^2
$S_{\Delta\Delta,qmn,q'm'n'}$	=	modal cross power spectral density of the pressure jump, Pa^2.s.rad^{-1}
S_{pp}	=	power spectral density of the far-field radiated pressure, Pa^2.s.rad^{-1}
$S_{QQ,qmn}$	=	modal cross power spectral density of the unsteady lift, N^2.s.rad^{-1}
s_i	=	airfoil sweep distance, m
T	=	averaging time, s
t	=	observer time, s
$\mathbf{U}_{\phi i}$	=	ith rotor tangential speed, m.s^{-1}
$\mathbf{U}_{X1}$	=	front airfoils freestream velocity in the chordwise direction, m.s^{-1}
$\overline{u^2}$	=	mean square turbulent velocity fluctuation, m^2.s^{-2}
$\mathcal{W}$	=	upwash velocity of isotropic homogeneous turbulence in wavenumber domain, m^4.s^{-1}
W	=	mean gust velocity in the rotating reference frame $\tilde{\mathbf{X}}_2$, m.s^{-1}
w	=	upwash velocity of isotropic homogeneous turbulence, m.s^{-1}
w_W	=	upwash velocity of turbulent wakes, m.s^{-1}
$\mathbf{X}_i = (r, X_i, Y_i)$	=	cylindrical coordinate bound to an airfoil, in radial, chordwise and normal directions
$\mathbf{x} = (x, y, z)$	=	Cartesian coordinate system bound to the engine
$\mathbf{x}_0 = (r_0, \theta, \psi_0)$	=	spherical coordinate system for far-field observer
$\mathbf{x}_i = (r, x_i, \phi_i)$	=	cylindrical coordinate bound to an airfoil, in radial, axial and azimuthal directions
α_i	=	blade stagger angle, rad
Δl_r	=	spanwise correlation length of the unsteady blade loading, m
Δr_j	=	strip width, m
Δp	=	pressure jump across the rear airfoils, kg.m^{-1}.s^{-2}
η, η_0	=	absolute and normalized rotor–rotor gap, m and nondimensional
κ_{qmn}	=	aeroacoustic coupling wavenumber, m^{-1}
ω	=	angular frequency, rad.s^{-1}
Ω_i	=	rotor angular speed, rad.s^{-1}
ω_{qmn}	=	interaction angular frequency, rad.s^{-1}
Φ_{ww}	=	wavenumber spectrum of the turbulent upwash velocity, m^5.s^{-2}
Π_{ml}	=	modal radiation term, m^{-4}
ψ_2	=	azimuthal correction for the chordwise location of the source, rad
ρ_0	=	density of air, kg.m^{-3}

Received 22 March 2010; revision received 28 June 2010; accepted for publication 4 July 2010.

*Research Student, Fluid Dynamics and Acoustics Group, Institute of Sound and Vibration Research.

†Professor of Engineering Acoustics, Fluid Dynamics and Acoustics Group, Institute of Sound and Vibration Research.

τ = source emission time, s
$\breve{(.)}$ = quantity expressed following Chapman's similarity rule
$\hat{(.)}$ = quantity expressed in the frequency domain
$(.)_i$ = $i = 1, 2$ denotes a quantity associated to the front or rear rotor respectively
$[.]_t$ = quantity expressed at observer time
$\langle . \rangle$ = expected value
$\tilde{(.)}$ = quantity in a rotating reference frame fixed to a blade

I. Introduction

THERE has been growing interest in contra-rotating open rotors (CRORs, see Fig. 1) as an alternative to turbofan engines for use as the power plants on aircraft. They are estimated to burn 20–30% less fuel than equivalent turbofan engines for short-haul flights. However, one of the main challenges for their introduction, which led to the rejection of the concept in the late 1980s, is their very high levels of noise emissions. There is therefore a need for schemes by which the noise from CRORs can be predicted and hence reduced. Semi-analytical methods for the prediction of tonal noise of CRORs are already in existence, see for example Hanson [1], Parry [2,3], Parry and Crighton [4], and Whitfield et al. [5], but, to the authors' knowledge, no prediction schemes and very little measurements of the broadband noise from CRORs are available in the literature.

CRORs are complex aeroacoustic systems in which various sources of tonal and broadband noise are present. They exhibit a strong tonal signature over a wide frequency range compared with single propellers and turbofans. All of the early work has therefore focused on tonal noise, while broadband noise emissions from CRORs remain poorly understood. Furthermore, there is a lack of published broadband noise measurements from CRORs. It is therefore difficult to predict a priori which aerodynamic processes are significant to the overall radiation of broadband noise. Nevertheless, possible broadband noise sources can be identified by analogy with broadband noise generation from ducted turbofans, see for example [6] (chapter 3) for details. The dominant broadband noise source from CRORs is believed to be due to the interaction between the turbulent wakes shed from the front rotor and the rear rotor. This mechanism is therefore the subject of this paper.

The model of CROR broadband noise presented here combines Hanson's [1] semi-analytical scheme for tonal noise prediction with the classical theory for the unsteady loading of isolated unloaded flat plates in a turbulent stream, based on the work of Amiet [7]. In this paper, an expression is derived for the sound power level (PWL) radiated to a far-field observer from a stationary CROR (i.e., wind-tunnel configuration). Because the solidity of CRORs is generally low, single-airfoil blade response theory is used to predict the unsteady loading over the rear rotor blades (see [8,9]), assuming that the airfoils are thin unloaded flat plates. Turbulent wake parameters are deduced from mean aerodynamic quantities using the empirical correlations proposed by Gliebe et al. [10]. The wake turbulence is assumed to be homogeneous and isotropic, which is modulated by a periodic train of wake profiles. Strip theory is used to treat the spanwise variation in aerodynamic parameters and geometry.

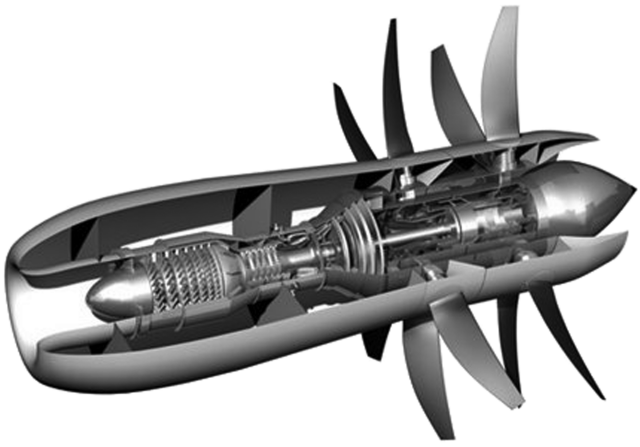

Fig. 1 Example of a contrarotating open rotor in pusher configuration. Credit: Rolls-Royce plc.

The model presented here is a modified and corrected version of the model introduced in [11], by the authors of this paper. The original model in [11] relates to a CROR flying over a stationary observer in the far field. A factor $1/\pi$ was missing in equation 33 of [11], but this has been corrected in the current paper. It was shown in [11] that the broadband noise model significantly under-predicted the experimental data measured on a model-scale CROR in the late 1980s. However, we have since learned that the experimental data may not be reliable as it was measured in the lined working section of a closed wind tunnel in which reverberation and flow noise are present. Agreement of better than 5 dB has since been obtained between model presented here and recent noise measurements on a model-scale fan rig. However, these comparisons are confidential at the time of writing.

As demonstrated by Casper and Farassat [12], the expression for the pressure jump due to a stochastic velocity input can also be formulated in the time domain. Farassat et al. [13] have also shown that the unsteady blade loading can be computed efficiently in the time domain for airfoils with real blade geometry (e.g., finite camber and thickness), forward motion effects and supersonic helical tip speeds. Whilst time domain methods offer certain computational advantages, the current frequency domain approaches reveals explicitly the subtle effects of frequency scattering due to the two rotors rotating in opposite directions.

One of the most questionable simplifying assumptions made in this paper is of representing the unsteady blade response by those from unloaded flat plates. Recent work by, for example, Devenport et al. [14] has demonstrated, by comparison of the measured noise from real airfoils with noise predictions based on flat-plate theory, that angle of attack has only a small effect on leading edge noise because of the averaging effect of the isotropic turbulence spectrum. Angle of attack effects can, however, be significant in nonisotropic turbulence and dependent on airfoil shape. It was found that thicker airfoils generate significantly less noise at high frequencies. Camber effects were found to be small, however.

II. Broadband Noise from Rotor-Wake/Rotor Interaction in CRORs

A. Model Description

1. 2D Representation of Rotor-Wake/Rotor Interaction

Turbulent wakes are shed from the trailing edge of the front rotor and convected in a helical motion onto the leading edge of the rear rotor. This impingement of the wake turbulence generates a stochastic unsteady loading on the rear rotor blades that radiates as broadband noise.

Figure 2 presents a 2D representation of the rotor–wake/rotor interaction problem and introduces the main geometrical parameters of the model. At any radial position r, the front and rear rotors are represented by two infinite cascades of flat plates of chords c_1 and c_2, with stagger angles α_1 and α_2, rotating at speeds $\mathbf{U}_{\phi 1} = r\Omega_1 \mathbf{e}_{\phi 1}$ and $\mathbf{U}_{\phi 2} = r\Omega_2 \mathbf{e}_{\phi 2}$, respectively. The blades are separated azimuthally by the gaps $d_1 = 2\pi r/B_1$ and $d_2 = 2\pi r/B_2$. The distance η is the axial separation between the midchord disks of the two rotors at the hub. In the rest of this paper, the subscripts $(.)_i$, with $i = 1$ or 2, denote quantities associated with the front or rear rotor, respectively.

The coordinate systems $(\mathbf{e}_r, \mathbf{e}_{xi}, \mathbf{e}_{\phi i})$ and $(\mathbf{e}_r, \mathbf{e}_{Xi}, \mathbf{e}_{Yi})$ are defined in Fig. 2 and are related to each other by a rotation equal to the stagger angle α_i. They are associated with the rotating reference frames $\tilde{\mathbf{x}}_i = (r, \tilde{x}_i, \tilde{\phi}_i)$ and $\tilde{\mathbf{X}}_i = (r, \tilde{X}_i, \tilde{Y}_i)$, fixed on the midchord of a reference blade. In this paper, the tilde $\tilde{(.)}$ denotes a quantity expressed in a rotating reference frame fixed to a blade. To express the broadband noise radiated to the far-field, two reference frames bound to the engine are defined as $\mathbf{x}_i = (r, x_i, \phi_i)$ and $\mathbf{X}_i = (r, X_i, Y_i)$. The

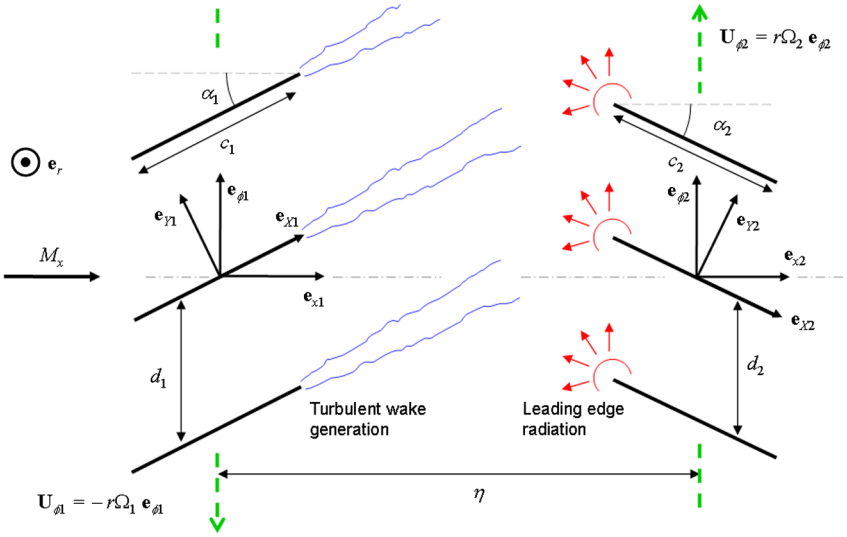

Fig. 2 Rotor–wake/rotor interaction in a 2D slice of a CROR, unrolled at radius r.

engine-bound and rotating airfoil-bound reference frames can be related through $\tilde{\phi}_1 = \phi_1 + \Omega_1\tau$ and $\tilde{\phi}_2 = \phi_2 - \Omega_2\tau$, where τ is the source emission time.

Figure 3 defines the mean gust velocity $\mathbf{W}$ in the rear airfoil-bound rotating coordinate system $\tilde{\mathbf{X}}_2$. An observer in the reference frame $\tilde{\mathbf{X}}_1$, rotating with the front airfoils, will see a fluid particle just outside the wake leaving the first blade row in the chordwise direction $\mathbf{e}_{X1}$ with a velocity $\mathbf{U}_{X1}$. However, in the engine-bound reference frame, the wake follows a helical path and the same fluid particle will be convected towards the rear blade row with a mean velocity $\mathbf{U}_{\text{obs}}$. In the reference frame $\tilde{\mathbf{X}}_2$, bound to a rear airfoil, the resulting unsteady turbulent gust has a mean velocity $\mathbf{W}$, defined as the resultant of the mean velocity $\mathbf{U}_{X1}$ and the sum of the rotational azimuthal velocities $\mathbf{U}_{\phi 1} - \mathbf{U}_{\phi 2} = -r(\Omega_1 + \Omega_2)\mathbf{e}_{\phi 2}$, and which may be expressed as

$$\mathbf{W} = r(\Omega_1 + \Omega_2)\frac{\cos\alpha_1}{\sin(\alpha_1 + \alpha_2)}\mathbf{e}_{X2} \tag{1}$$

Broadband noise due to leading edge interaction is known to be weakly dependent on the angle of attack of the airfoil provided that the angle of attack is roughly less than 10° (see for example Devenport et al. [14]). Therefore, steady blade loading is neglected and the relative gust velocity $\mathbf{W}$ is assumed to be parallel to the chord of the rear blade row.

2. *Radiation to the Far Field*

To specify the location of an acoustic source on the blade surface with respect to a far-field observer, two additional coordinate systems must be introduced: a spherical coordinate system $\mathbf{x}_0 = (r_0, \theta, \psi_0)$ denoting the location of the observer with respect to the engine, and a Cartesian coordinate system $\mathbf{x} = (x, y, z)$ denoting the location of an acoustic point source on a blade with respect to the engine body. These are defined in Fig. 4a, where M_x is the axial flow Mach number in the engine-bound reference frame, M_{t2} is the rear rotor tip Mach number and $d\mathbf{F}$ is the elementary force applied by a surface element of the blade to the fluid. As shown in Fig. 4b, an additional azimuthal angle $\psi_2 = -(X_2 + s_2)\sin\alpha_2/r$ is introduced to take into account the chordwise position of the source and the airfoil radial sweep s_2.

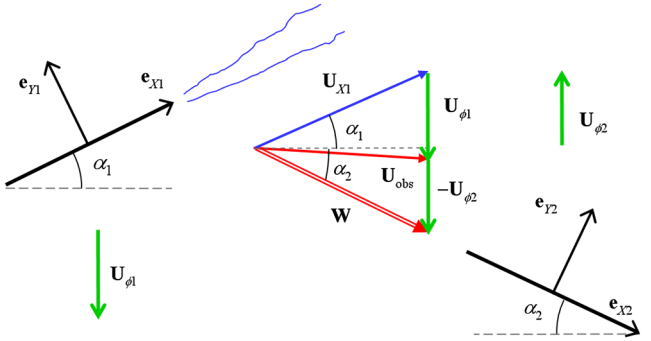

Fig. 3 Definition of the relative mean gust velocity W in the airfoil-bound reference frame $\tilde{\mathbf{X}}_2 = (\tilde{r}_2, \tilde{X}_2, \tilde{Y}_2)$.

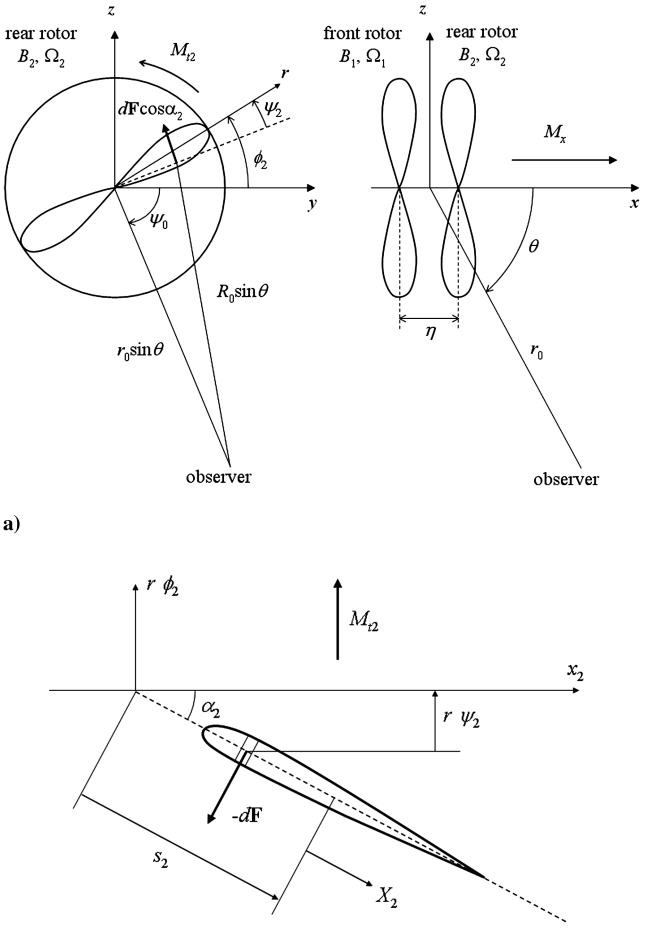

Fig. 4 Coordinate systems for a) an observer in the far field, and b) a point force on a swept blade of the downstream rotor.

Making the far-field approximation allows the distance between the source and observer R_0 to be approximated by r_0 in the amplitude terms, but further accuracy is required in the phase terms to properly take account of the rotation of the source. The following first order Taylor decomposition of R_0, obtained after some manipulation of the coordinate systems, is therefore used in the phase terms

$$R_0 \approx r_0 - (X_2 + s_2)\cos\alpha_2 \cos\theta - r\sin\theta\cos(\phi_2 - \psi_2 + \psi_0) \quad (2)$$

B. Analytical Formulation

1. Turbulent Wake Model

The model of the turbulent wake velocity follows an approach similar to, for example, Jurdic et al. [15]. The turbulent velocity component of the wakes normal to the blades (or upwash velocity) w_W can be expressed in the reference frame $\tilde{\mathbf{X}}_2$ rotating with the rear rotor as a velocity w, that is a random function of space and time, modulated by a deterministic nondimensional wake profile function f_W as

$$w_W(\tilde{\mathbf{X}}_2, \tau) = f_W(\tilde{\mathbf{X}}_2, \tau) w(\tilde{\mathbf{X}}_2, \tau) \quad (3)$$

The random function $w(\tilde{\mathbf{X}}_2, \tau)$ is assumed to have the same spectral and spatial correlation characteristics as the turbulence, which is assumed to be isotropic and homogeneous. The wake profile function $f_W(\tilde{\mathbf{X}}_2, \tau)$ is chosen in this study to be a periodic train of Gaussian profiles. This wake turbulence model has been validated recently by Jurdic et al. [16], who used cyclostationary spectral analysis on measurements of rotor–wake turbulence on a rig. Assuming that the profile of a turbulent wake repeats identically in the azimuthal direction $\mathbf{e}_{\phi 1}$, at every blade separation $d_1 = 2\pi r/B_1$, the wake profile function f_W can be expressed as

$$f_W(\tilde{\mathbf{X}}_2, \tau) = \sum_{k=-\infty}^{\infty} \exp\left\{-\frac{a}{b_W^2}((\tilde{\mathbf{X}}_2 - \mathbf{W}\tau) .(\mathbf{e}_{\phi 1} - \mathbf{e}_{x1}\tan\alpha_1) + k d_1)^2\right\} \quad (4)$$

where b_W is the half-wake width and where a is an empirical wake parameter set to $a = 0.637$ by Wygnanski et al. [17] from laboratory measurements of 2D turbulent wakes. In the absence of wake turbulence measurements, the mean and turbulent wake parameters can be deduced from the mean streamwise velocity U_{X1} and the drag coefficient of the front airfoils C_d using the empirical correlations of Gliebe et al. [10].

The wake turbulence model described in Eq. (3), which is based on the work of Ventres et al. [18] for the prediction of the broadband noise due to rotor–stator interactions in turbofans (and subsequently used in [15,19,20]), is fundamentally limited to well separated wakes. If the wake width $2b_W$ is not small compared with the blade gap d_1, adjacent wakes will overlap, leading to a correlation between adjacent front blades that cannot occur in practice as adjacent turbulent wakes must be statistically independent. The use of Eq. (3) for overlapping wakes will, therefore, yield an unrealistic scaling of the mean square acoustic pressure with B_1^2. To the knowledge of the authors, this limitation has not been previously recognized. The condition $d_1/2b_W > 1$ is therefore necessary for the current approach to be valid. This condition is, however, generally valid for most realistic configurations of CRORs, due to the low drag coefficient of the front blades (i.e., thin wakes) and the low number of front blades B_1 (i.e., large blade separation).

To derive an expression for the turbulent upwash velocity, we consider the velocity of the wake turbulence as a frozen pattern independent of τ in the reference frame moving with the gust at a velocity $\mathbf{W}$ (Taylor's hypothesis). The resulting frozen upwash velocity is defined by $\tilde{w}_W(\tilde{\mathbf{X}}_2 - \mathbf{W}\tau) = w_W(\tilde{\mathbf{X}}_2, \tau)$. Applying Poisson's summation formula to Eq. (4) and substituting the result into Eq. (3) yields

$$\tilde{w}_W(\tilde{\mathbf{X}}_2 - \mathbf{W}\tau) = \sum_{m=-\infty}^{\infty} f_m(r)\tilde{w}(\tilde{\mathbf{X}}_2 - \mathbf{W}\tau) e^{-i\frac{mB_1}{r}(\tilde{\mathbf{X}}_2 - \mathbf{W}\tau).(\mathbf{e}_{\phi 1} - \mathbf{e}_{x1}\tan\alpha_1)} \quad (5)$$

where the index m denotes the mth harmonic of the blade passing frequency $mB_1\Omega_1/2\pi$ (in Hz) of the front rotor and where f_m are the Fourier components of the wake profile given by

$$f_m(r) = \frac{1}{\sigma\sqrt{2\pi}}\exp\left\{-\frac{1}{2}\left(\frac{m}{\sigma}\right)^2\right\} \quad (6)$$

with $\sigma = \frac{r\sqrt{2a}}{B_1 b_W}$. Equation (6) suggests that the energy of the upwash velocity is distributed over the indices m following a Gaussian distribution centered at $m = 0$ with "standard deviation" σ.

The turbulent velocity w can be expressed in terms of its wavenumber Fourier transform as

$$\tilde{w}(\tilde{\mathbf{X}}_2 - \mathbf{W}\tau) = \frac{1}{(2\pi)^3}\iint_{-\infty}^{\infty}\int \mathcal{W}(\mathbf{k}) e^{-i\mathbf{k}.(\tilde{\mathbf{X}}_2 - \mathbf{W}\tau)}\,\mathrm{d}\mathbf{k} \quad (7)$$

where $\mathbf{k} = (k_r, k_X, k_Y)$ denotes the turbulence wavenumber vector and $\mathcal{W}$ the wavenumber velocity spectrum, both expressed in the reference frame moving with the turbulent gust $\tilde{\mathbf{X}}_2 - \mathbf{W}\tau$.

To consider the unsteady loading on the rear rotor, the upwash velocity must be expressed in the coordinate system $\tilde{\mathbf{x}}_2 = (r, \tilde{x}_2, \tilde{\phi}_2)$ to make explicit the dependence on azimuthal coordinate $\tilde{\phi}_2$. Substituting Eq. (1) into Eq. (5) and expanding the dot product in the exponent yields

$$\begin{aligned} w_W(r, \tilde{x}_2, \tilde{\phi}_2, \tau) = {} & \frac{1}{(2\pi)^3}\sum_{m=-\infty}^{\infty} f_m(r) \\ & \times \iint_{-\infty}^{\infty}\int \mathcal{W}(k_r, k_X, k_Y) e^{-i[(k_\phi + \frac{mB_1}{r})r\tilde{\phi}_2 + mB_1(\Omega_1 + \Omega_2)\tau]} \\ & \times e^{-i[k_r r + (k_x - \frac{mB_1}{r}\tan\alpha_1)\tilde{x}_2 - k_X W\tau]}\,\mathrm{d}k_r\,\mathrm{d}k_X\,\mathrm{d}k_Y \end{aligned} \quad (8)$$

where k_ϕ and k_x are the turbulent wavenumbers in the azimuthal and axial directions, respectively, and are given by

$$\begin{cases} k_\phi = -k_X\sin\alpha_2 + k_Y\cos\alpha_2 \\ k_x = k_X\cos\alpha_2 + k_Y\sin\alpha_2 \end{cases} \quad (9)$$

Equation (8) is an expression for the upwash turbulent velocity in the reference frame rotating with the rear rotor. In the next section, this expression is used to deduce the unsteady loading on the B_2 blades of the rear rotor.

2. Unsteady Loading on the Rear Rotor from Isolated Flat-Plate Theory

The expression for the unsteady loading on the rear blade row is now presented. According to Amiet [7], the unsteady pressure difference Δp (or pressure jump) across an isolated airfoil due to a harmonic vortical gust, with upwash velocity of the form $w(r, X_2, Y_2, \tau) = w_0 e^{-i[k_r r + k_X(X_2 - W\tau) + k_Y Y_2]}$, can be written as

$$\begin{aligned} & \Delta p(r, X_2, Y_2, k_r, k_X, k_Y, \tau) \\ & \quad = 2\pi\rho_0 W w_0 g(X_2, k_r, k_X, M_W) e^{-i[k_r r + k_Y Y_2 - k_X W\tau]} \end{aligned} \quad (10)$$

where $M_W = W/c_0$ is the Mach number of the relative mean flow onto the leading edge of the airfoil and $g(X_2, k_r, k_X, M_W)$ is the nondimensional transfer function between the turbulent upwash velocity and the pressure jump. In this study, the flat-plate response functions g derived by Amiet [8,9] are used, following the same approach as [21]. The pressure jump across an arbitrary reference airfoil of the rear rotor, expressed in an airfoil-bound rotating reference frame, is denoted by $\Delta\tilde{p}$. The expression for $\Delta\tilde{p}$ is obtained by substituting the turbulent upwash velocity w_W [Eq. (8)], estimated at the leading edge of the reference airfoil, into the general formula of Eq. (10) and integrating over all turbulence wavenumber components. Noting that on the surface of the flat plate one can make

the change of variables $\tilde{x}_2 = (\tilde{X}_2 + s_2)\cos\alpha_2$, $\Delta\tilde{p}$ is expressed in the coordinate system $(r, \tilde{X}_2, \tilde{\phi}_2)$ as

$$\begin{aligned}\Delta\tilde{p}(r,\tilde{X}_2,\tilde{\phi}_2,\tau) &= \frac{1}{(2\pi)^2}\rho_0 W\sum_{m=-\infty}^{\infty} f_m(r)\\ &\times \iint_{-\infty}^{\infty}\int \mathcal{W}(k_r,k_X,k_Y)g(\tilde{X}_2,k_r,k_X,M_W)\\ &\times e^{-i[(k_\phi+\frac{mB_1}{r})r\tilde{\phi}_2+(mB_1(\Omega_1+\Omega_2)-k_X W)\tau]}\\ &\times e^{-i[k_r r-(s_2+\tilde{X}_2)\frac{mB_1}{r}\tan\alpha_1\cos\alpha_2]}\,\mathrm{d}k_r\,\mathrm{d}k_X\,\mathrm{d}k_Y \end{aligned} \tag{11}$$

The source of broadband noise, specified by the pressure jump across the rear rotor blades, must be expressed in the engine-bound reference frame (r, X_2, ϕ_2) before the far-field noise can be calculated. By considering the rear rotor loading as a series of pulses repeating every B_2 blades, the pressure jump $\Delta p(r, X_2, \phi_2)$ is deduced from $\Delta\tilde{p}(r, \tilde{X}_2, \tilde{\phi}_2, \tau)$ as

$$\begin{aligned}\Delta p(r,X_2,\phi_2,\tau) &= \sum_{n=-\infty}^{\infty}\Delta\tilde{p}(r,\tilde{X}_2,\tilde{\phi}_2,\tau)\delta\left(\tilde{\phi}_2-\frac{2\pi}{B_2}n\right)\\ &= \frac{B_2}{2\pi}\sum_{n=-\infty}^{\infty}\Delta\tilde{p}(r,\tilde{X}_2,\tilde{\phi}_2,\tau)e^{\mathrm{i}nB_2\tilde{\phi}_2}\end{aligned} \tag{12}$$

where δ is the Dirac delta function and where the right hand side expression has been obtained using Poisson's summation formula.

Following the approach of Hanson and Horan [22], the turbulence velocity is assumed 2π-periodic at a fixed instant in time, and the turbulent velocity field is decomposed in the azimuthal direction as a sum of Fourier modes of order q. The turbulent azimuthal wavenumber k_ϕ therefore only takes the discrete values

$$k_\phi = k_Y\cos\alpha_2 - k_X\sin\alpha_2 = -\frac{2\pi q}{B_2 d_2} = -\frac{q}{r} \tag{13}$$

Equation (13) leads to a direct relationship between the normal and chordwise turbulent wavenumbers k_Y and k_X

$$k_Y = k_X\tan\alpha_2 - \frac{q}{r\cos\alpha_2} \tag{14}$$

It will be later shown that k_X is constant at a single frequency. As a consequence, the k_Y integral in Eq. (11) can be expressed as a summation using

$$\int_{-\infty}^{\infty}\mathrm{d}k_Y \to \frac{1}{r\cos\alpha_2}\sum_{q=-\infty}^{\infty} \tag{15}$$

because $\Delta q = 1$. Combining Eqs. (11–15) yields an expression for the pressure jump in the engine-bound reference frame as

$$\begin{aligned}\Delta p(r,X_2,\phi_2,\tau) &= \frac{1}{(2\pi)^3}\frac{\rho_0 W B_2}{r\cos\alpha_2}\sum_{q=-\infty}^{\infty}\sum_{m=-\infty}^{\infty}\sum_{n=-\infty}^{\infty} f_m(r)\\ &\times\int_{-\infty}^{\infty}\int_{-\infty}\mathcal{W}(k_r,k_X,k_Y)g(X_2,k_r,k_X,M_W)\\ &\times e^{-i[l\phi_2+k_r r-\frac{mB_1}{r}\tan\alpha_1\cos\alpha_2(X_2+s_2)+(\omega_{qmn}-k_X W)\tau]}\,\mathrm{d}k_r\,\mathrm{d}k_X\end{aligned} \tag{16}$$

where the azimuthal acoustic interaction mode l and the interaction frequency ω_{qmn} are defined by

$$l = mB_1 - (nB_2 + q) \tag{17}$$

$$\omega_{qmn} = mB_1\Omega_1 + (nB_2 + q)\Omega_2 \tag{18}$$

Equation (17) establishes the scattering rule linking the acoustic mode, of order l, resulting from the interaction between the qth turbulent mode originating from B_1 wakes and the B_2 blades of the downstream rotor. Because the engine is not moving with respect to the observer (i.e., wind-tunnel configuration), the relationship between the emission time τ and the observer time t is

$$\tau = t - R_0/c_0 \tag{19}$$

Substituting the relationship between R_0 and r_0 [Eq. (2)] for the phase terms and the retarded time [Eq. (19)] into Eq. (16) yields the expression for the pressure jump at the observer time t. Now performing a Fourier transform with respect to observer time t yields the expression for the frequency domain pressure jump $\Delta\hat{p}$, for a far-field stationary observer, given by

$$\begin{aligned}\Delta\hat{p}(r,X_2,\phi_2,\omega) &= \frac{1}{(2\pi)^2}\frac{\rho_0 B_2}{r\cos\alpha_2}\sum_{q=-\infty}^{\infty}\sum_{m=-\infty}^{\infty}\sum_{n=-\infty}^{\infty} f_m(r)\\ &\times e^{-i[k_0 r_0-(\frac{mB_1}{r}\tan\alpha_1\cos\alpha_2+k_0\cos\alpha_2\cos\theta)(X_2+s_2)-k_0 r\sin\theta\cos(\phi_2-\psi+\psi_0)]}\\ &\times e^{-il\phi_2}\int_{-\infty}^{\infty}\mathcal{W}(k_r,K_{X,qmn},K_{Y,qmn})g(X_2,k_r,K_{X,qmn},M_W)e^{-ik_r r}\,\mathrm{d}k_r\end{aligned} \tag{20}$$

where $k_0 = \omega/c_0$ and the convention $\hat{(.)}$ denotes a quantity in the frequency domain. Note that, following Fourier transformation with respect to t, the k_X integral in Eq. (16) vanishes and, at a given frequency, the turbulent wavenumbers k_X and k_Y now take the discrete values

$$K_{X,qmn} = \frac{\omega+\omega_{qmn}}{W} \quad\text{and}\quad K_{Y,qmn} = K_{X,qmn}\tan\alpha_2 - \frac{q}{r\cos\alpha_2} \tag{21}$$

The expression for the pressure jump in Eq. (20) quantifies the strength of the equivalent acoustic dipole source distribution on the rear rotor blades from the point of view of an observer in the far-field. It can now be input into the Ffowcs-Williams and Hawkings equation ([23]) to predict the radiated far-field spectrum, as described in the next section.

3. *Sound Pressure Spectral Density*

The derivation of the expression for broadband noise spectrum of far-field noise radiation is now presented. The acoustic pressure p due to a moving elementary force $d\mathbf{F}$ (of unit $\mathrm{N.m^{-2}}$) exerted by a blade surface element (of area $\mathrm{d}S_2$) on the fluid is given by the Ffowcs-Williams and Hawkings [23] equation as

$$p(\mathbf{x}_0,t) = -\int_{S_2}\nabla\cdot\left[\frac{d\mathbf{F}(\mathbf{x}_2,\tau)}{4\pi R_0}\right]_t \mathrm{d}S_2(\mathbf{x}_2) \tag{22}$$

where R_0 is the distance between the observer at time t and the source at time τ. The observer and source position vectors, $\mathbf{x}_0$ and $\mathbf{x}_2$, are defined in Sec. II.A, S_2 denotes the surface of the rear rotor blades and the square brackets $[.]_t$ denote an estimation at observer time t. As stated in Sec. II.A.2., the $1/R_0$ amplitude term can be approximated by $1/r_0$.

Noting that the magnitude dF of the elemental force is directly linked to the pressure jump over the airfoil as $dF = -\Delta p$, using the definition of the elemental force vector (see Fig. 4) and Eq. (20), the divergence of the moving point force for a single value of (m, n, q) can be derived in the frequency domain as

$$\begin{aligned}&\nabla\cdot d\hat{\mathbf{F}}_{qmn}(r,X_2,\phi_2,\omega)\\ &\quad= i\left(\frac{l}{r}\cos\alpha_2 + k_0\sin\alpha_2\cos\theta\right)\Delta\hat{p}_{qmn}(r,X_2,\phi_2,\omega)\end{aligned} \tag{23}$$

The far-field acoustic pressure spectrum is then obtained by substituting Eqs. (22) and (23) to give

$$\begin{aligned}\hat{p}_{qmn}(r_0,\theta,\psi_0,\omega) &= -i\int_{R_{h2}}^{R_{t2}}\int_{-c_2/2}^{c_2/2}\int_0^{2\pi}\frac{(\frac{l}{r}\cos\alpha_2 + k_0\cos\theta\sin\alpha_2)}{4\pi r_0}\\ &\times\Delta\hat{p}_{qmn}(r,X_2,\phi_2,\omega)\,\mathrm{d}\phi_2\,\mathrm{d}X_2\,\mathrm{d}r\end{aligned} \tag{24}$$

where R_{h2} and R_{t2} denote the radii of the hub and the tip of the rear rotor, respectively.

The integration over ϕ_2 is derived analytically by extracting the ϕ_2-dependent part from $\Delta\hat{p}_{qmn}(r, X_2, \phi_2, \omega)$ [Eq. (20)] as

$$\int_0^{2\pi} e^{ik_0 r\sin\theta\cos(\phi_2-\psi+\psi_0)+il\phi_2}\,\mathrm{d}\phi_2 = 2\pi e^{il(\psi_0+\frac{\pi}{2})} e^{i\frac{l}{r}\sin\alpha_2(X_2+s_2)} J_l(k_0 r\sin\theta) \tag{25}$$

Substituting Eq. (20) into Eq. (24) and using the identity of Eq. (25) yields the final expression for the single frequency far-field pressure of the form

$$\begin{aligned}\hat{p}_{qmn}(r_0,\theta,\psi_0,\omega) &= \frac{-i}{8\pi^2}\frac{\rho_0 c_2 B_2}{2r_0} e^{-i[k_0 r_0 - l(\psi_0+\pi/2)]} \\ &\times \int_{R_{h2}}^{R_{t2}} f_m(r)\left(\frac{l}{r}+k_0\cos\theta\tan\alpha_2\right)\frac{J_l(k_0 r\sin\theta)}{r} \\ &\times \int_{-\infty}^{\infty} \mathcal{W}(k_r, K_{X,qmn}, K_{Y,qmn}) L_{qmn}(k_r, K_{X,qmn}, \kappa_{qmn}) e^{-ik_r r}\,\mathrm{d}k_r\,\mathrm{d}r\end{aligned} \tag{26}$$

where L_{qmn} denotes the nondimensional aerodynamic-acoustic coupling integral along the airfoil and is defined by

$$L_{qmn}(k_r, K_{X,qmn}, \kappa_{qmn}) = \frac{2}{c_2}\int_{-c_2/2}^{c_2/2} g(X_2, k_r, K_{X,qmn}, M_W) e^{i\kappa_{qmn}(X_2+s_2)}\,\mathrm{d}X_2 \tag{27}$$

where κ_{qmn} is the aeroacoustic coupling wavenumber given by

$$\kappa_{qmn} = k_0\cos\alpha_2\cos\theta + mB_1\frac{\Omega_1+\Omega_2}{W} - \frac{nB_2+q}{r}\sin\alpha_2 \tag{28}$$

The chordwise integral L_{qmn} includes noncompactness effects and can be interpreted as a coupling integral between the unsteady aerodynamics and the acoustic radiation to the far field. A maximum of $|L_{qmn}|$ is obtained when both the vortical chordwise wavenumber $K_{X,qmn}$ and the aeroacoustic coupling wavenumber κ_{qmn} tend to zero. The expression for L_{qmn} has been derived analytically using the classical approach of Amiet [21].

Because aerodynamic broadband noise involves stochastic quantities, such as the turbulent upwash velocity, the broadband far-field noise must be evaluated as a spectral density. The power spectral density (PSD) of the far-field acoustic pressure can be derived from $S_{pp} = \lim_{T\to\infty}\frac{\pi}{T}\langle\hat{p}\hat{p}^*\rangle$, where the brackets $\langle.\rangle$ denote the expected value and T represents the averaging time. Its contribution from (m, n, q) and (m', n', q'), is obtained from Eq. (24) as

$$\begin{aligned}S_{pp,qmn,q'm'n'}(r_0,\theta,\omega) &= \left(\frac{1}{4\pi r_0}\right)^2 \int_{R_{h2}}^{R_{t2}}\int_{-\frac{c_2}{2}}^{\frac{c_2}{2}}\int_0^{2\pi}\int_{r-\frac{\Delta L_r}{2}}^{r+\frac{\Delta L_r}{2}}\int_{-\frac{c_2}{2}}^{\frac{c_2}{2}}\int_0^{2\pi} \\ &\times S_{\Delta\Delta,qmn,q'm'n'}\left(\frac{l'}{r}\cos\alpha_2 + k_0\cos\theta\sin\alpha_2\right) \\ &\times \left(\frac{l}{r}\cos\alpha_2 + k_0\cos\theta\sin\alpha_2\right)\mathrm{d}r\,\mathrm{d}X_2\,\mathrm{d}\phi_2\,\mathrm{d}r'\,\mathrm{d}X_2',\ \mathrm{d}\phi_2'\end{aligned} \tag{29}$$

where $S_{\Delta\Delta,qmn,q'm'n'}$ is the modal cross-PSD of the pressure jump between two points (r, X_2, ϕ_2) and (r', X_2', ϕ_2') on the blade surface and is defined by

$$S_{\Delta\Delta,qmn,q'm'n'}(r, X_2, \phi_2, r', X_2', \phi_2', \omega) = \lim_{T\to\infty}\frac{\pi}{T}\langle\Delta\hat{p}^*_{qmn}(r, X_2, \phi_2, \omega)\Delta\hat{p}_{q'm'n'}(r', X_2', \phi_2', \omega)\rangle \tag{30}$$

Two sources of broadband noise on a rear rotor blade can be considered uncorrelated if their radial separation is larger than the spanwise correlation length Δl_r of the unsteady blade loading. Therefore, the domain of integration of the spanwise dr' integral in Eq. (29) has been restricted to $[r-\frac{\Delta L_r}{2},\ r+\frac{\Delta L_r}{2}]$, where ΔL_r is chosen to be sufficiently larger than Δl_r to ensure convergence of S_{pp}.

The only stochastic quantity in the expression for the pressure jump $\Delta\hat{p}$ [Eq. (20)] is $\mathcal{W}(k_r, k_X, k_Y)$. As a result, every other term can be written outside the expected value in Eq. (30), which can be simplified using Eq. (7). Assuming homogeneous turbulence gives

$$\langle\mathcal{W}^*(k_r, k_X, k_Y)\mathcal{W}(k_r', k_X', k_Y')\rangle = (2\pi)^3\delta(k_X-k_X')\delta(k_Y-k_Y')\delta(k_r-k_r')\Phi_{ww}(k_r', k_X', k_Y') \tag{31}$$

where Φ_{ww} is the turbulent velocity wavenumber spectrum, chosen to be the von Karman spectrum for isotropic and homogeneous turbulence (see for instance Amiet [7]), and is given by

$$\Phi_{ww}(k_r, k_X, k_Y) = \frac{55}{36\pi^{3/2}}\frac{\Gamma(5/6)}{\Gamma(1/3)}\frac{\overline{u^2}}{k_e^5}(k^2-k_Y^2)[1+(k/k_e)^2]^{-17/6} \tag{32}$$

where Γ is the gamma function, $k = \sqrt{k_r^2+k_X^2+k_Y^2}$ is the magnitude of the turbulence wavenumber vector, $\overline{u^2}$ is the mean square turbulent velocity fluctuation and k_e is defined by $k_e = \frac{\sqrt{\pi}}{L}\frac{\Gamma(5/6)}{\Gamma(1/3)}$.

To reduce the general expression of the PSD [Eq. (29)] to a form that is computationally more efficient, strip theory approximation is applied to account for the spanwise variation of aerodynamic quantities and geometry. Hence, the far-field pressure spectrum is assumed to be due to the sum of the contributions $S_{pp,j}$ generated by a distribution of N_j spanwise blade strips, whose flow and geometrical parameters are assumed to be uniform in each and equal to their value at the strip midspan. The span of each N_j strips, denoted by Δr_j, must be chosen to be larger than a turbulence integral lengthscale L, to encompass the largest scale eddies. The distance ΔL_r in Eq. (29) is chosen to be equal to the strip length Δr_j, its maximum value allowed by the use of strip theory, so that the condition $\Delta L_r = \Delta r_j > \Delta l_r$ is most likely to be satisfied.

Note that it is difficult to verify the validity of condition $\Delta r_j > \Delta l_r$, for the blade geometry and turbulent parameters under investigation here, since no simple expression for the correlation length Δl_r of the unsteady loading is available. However, the large-span approximation made later in this model overcomes this uncertainty. Further discussion about a relevant choice for Δl_r can be found in the work of Posson et al. [24].

Substituting Eq. (21) into Eq. (31) yields, after some analysis and for large values of T, the following identities

$$\begin{cases}\delta(K_{X,qmn} - K'_{X,q'm'n'}) = \frac{T}{\pi}W\delta_{m'm}\delta_{n'n}\delta_{q'q} \\ \delta(K_{Y,qmn} - K'_{Y,q'm'n'}) = r\cos\alpha_2\delta_{q'q}\end{cases} \tag{33}$$

where δ on the right hand side is the Kronecker delta function.

The spanwise separation distance $\delta r = r' - r$ is neglected in the amplitude terms of Eq. (26). Thus, combining the expression of the pressure jump [Eq. (20)] and the formulation for the PSD [Eq. (29) to Eq. (33)] yields the final expression of the PSD radiated by the jth strip of the form

$$S_{pp,j(r_0,\theta,\omega)} = \sum_{q=-\infty}^{\infty}\sum_{m=-\infty}^{\infty}\sum_{n=-\infty}^{\infty}\Pi_{ml}(r_0,\theta,\omega)S_{QQ,qmn}(\omega) \tag{34}$$

where $\bar{r}_j$ is the spanwise location of the midpoint of the jth strip, the radiation term Π_{ml} is defined as

$$\Pi_{ml}(r_0,\theta,\omega) = \left(\frac{B_2}{r_0}\right)^2 \int_{\bar{r}_j-\frac{\Delta r_j}{2}}^{\bar{r}_j+\frac{\Delta r_j}{2}}\frac{f_m^2(r)}{r\cos\alpha_2}\left(\frac{l}{r}\cos\alpha_2 + k_0\cos\theta\sin\alpha_2\right)^2 (J_l(k_0 r\sin\theta))^2\,\mathrm{d}r \tag{35}$$

and the modal cross-PSD $S_{QQ,qmn}$ of the unsteady blade loading is given by

$$S_{QQ,qmn}(\omega) = \frac{1}{4}\left(\rho_0 \frac{c_2}{2}\right)^2 W \int_{-\infty}^{\infty} \Phi_{ww}(k_r, K_{X,qmn}, K_{Y,qmn}) \times |L_{qmn}(k_r, K_{X,qmn}, \kappa_{qmn})|^2 \frac{\sin(k_r \frac{\Delta r_j}{2})}{\pi k_r} \, \mathrm{d}k_r \tag{36}$$

The expression for the PSD of the overall radiated noise is now reduced to a summation over N_j strips, each involving three infinite summations (over indices q, m and n) and two integrals over the strip span and the spanwise wavenumber. The term Π_{ml} and the cross-PSD $S_{QQ,qmn}$ of the unsteady loading, both appearing in Eq. (34), can be interpreted as a radiation term and a source term, respectively. The modal behavior of the radiated broadband noise is discussed in the next section.

The k_r integral in $S_{QQ,qmn}$ must be evaluated numerically and therefore represents a significant computational burden, which can be substantially reduced by making the large-span approximation. In the large-span limit, the identity

$$\lim_{\Delta r_j \to \infty} \frac{\sin(k_r \frac{\Delta r_j}{2})}{\pi k_r} = \delta(k_r) \tag{37}$$

can be used and, therefore, only small values of k_r contribute significantly to the radiated noise. Thus, in the large-span limit, Eq. (37) can be substituted into Eq. (36) to yield the following expression

$$S_{QQ,qmn}(r_0, \omega) = \frac{1}{4}\left(\rho_0 \frac{c_2}{2}\right)^2 W \Phi_{ww}(0, K_{X,qmn}, K_{Y,qmn}) |L_{qmn}(0, K_{X,qmn}, \kappa_{qmn})|^2 \tag{38}$$

This simplified form for the PSD of the broadband noise due to rotor–wake/rotor interaction may be used to establish the asymptotic behavior of the noise in the low- and high-frequency limits. In accordance with Eq. (32) for Φ_{ww}, the low and high-frequency asymptotic domains of Φ_{ww} are reached for $kL \ll 1$ and $kL \gg 1$, respectively. The summation over the indices q is equivalent to an integral over k_Y [see Eq. (15)], and the 3D velocity spectrum Φ_{ww} therefore varies with mean square velocity $\overline{u^2}$, integral length scale L and turbulent wavenumber magnitude k as a 2D spectrum. Assuming that $k \sim \omega/W$ and using the expression for the 2D von Karman wavenumber spectrum derived by Amiet [7], the low- and high-frequency scaling laws for Φ_{ww} can be expressed as $\lim_{kL\to 0}\Phi_{ww} \sim \overline{u^2} L^4 (\frac{\omega}{W})^2$ and $\lim_{kL\to\infty}\Phi_{ww} \sim \overline{u^2} L^{-2/3} (\frac{\omega}{W})^{-8/3}$, respectively. Because the flat-plate response functions of Amiet [8,9] are used and assuming that the frequencies of interest are not too low, the scaling of the unsteady loading term $|L_{qmn}|^2$ with flow speed and frequency can be approximated as $|L_{qmn}|^2 \sim \omega^{-2} W$. The scaling laws for the PSD of the broadband noise must also present a dependency on the half-wake width b_W, due to the Fourier components f_m^2 of the wake profiles appearing in Eq. (35). It can be seen from Eq. (6) that the term f_m^2 scales with b_W^2, but the fact the source term $S_{QQ,qmn}$ is summed over m yields a scaling of S_{pp} with b_W. Substituting the above scaling laws for Φ_{ww} and L_{qmn} into Eqs. (34), (35), and (38) yields the scaling laws of the PSD of the broadband noise due to rotor–wake/rotor interaction with $\overline{u^2}$, L, ω and W as

$$\lim_{kL\to 0} S_{pp} \sim b_W \overline{u^2} L^4 \omega^2 \qquad \lim_{kL\to\infty} S_{pp} \sim b_W \overline{u^2} L^{-2/3} W^{14/3} \omega^{-8/3} \tag{39}$$

The high-frequency scaling law in Eq. (39) is in agreement with the high-frequency approximated expression derived by Amiet [7], for predicting the broadband noise to an isolated flat plate in a turbulent stream. The scaling laws of Eq. (39) are verified in the parameter study presented in Sec. IV.

The derivation of the PWL, including the effects of a uniform mean flow, is detailed in Appendix A. The final expression is given by

$$\mathrm{PWL}\,(\omega) = 10\log_{10}\left(\frac{2\Pi(\omega)}{10^{-12}}\right), \qquad (\mathrm{dB}) \tag{40}$$

where

$$\Pi(\omega) = \frac{2\pi r_0^2}{\rho_0 c_0} \int_0^{\pi} S_{pp}(\check{r}_0, \check{\theta}, \psi_0, \omega) F(\theta, M_x) \sin\theta \, \mathrm{d}\theta \tag{41}$$

and where the function $F(\theta, M_x)$ is defined in Appendix A. The factor 2 in Eq. (40) has been introduced to consider only the positive frequencies of the spectrum. The term $S_{pp} = \sum_{j=1}^{N_j} S_{pp,j}$ in Eq. (41) is the total PSD of the broadband noise, obtained by summing the contribution $S_{pp,j}$ from all the N_j strips.

III. Modal Behavior of the Radiated Broadband Noise

In this section, a method for reducing the three infinite modal summations in the analytical expression of the PSD [Eq. (34)] is discussed. To identify the modes that contribute most significantly to the far-field radiation, it is essential to understand the variation of the modal PSD of the broadband noise $S_{pp,qmn} = \Pi_{ml} S_{QQ,qmn}$ [see Eqs. (35) and (38)], with m, n and q. In general, $S_{pp,qmn}$ varies slowly with changes in the turbulent mode order q but is highly sensitive to the value of the indices m and n. It is therefore proposed to investigate separately the behavior of $S_{pp,qmn}$ with the indices m and n and its behavior with the mode q.

A. Reduction of the Summations over the Scattering Indices *m* and *n*

Figure 5 shows the variation of the source term $S_{QQ,qmn}$ and radiation term Π_{ml} with the indices m and n for $q = 0$, for a single strip of the rear rotor at $\theta = 90°$ at $f = 8$ kHz. The configuration chosen here is that of a typical full-scale CROR. The source term $S_{QQ,qmn}$ can be seen to have energy distributed over a wide range of (m, n) but is mainly concentrated around the low values of the turbulent chordwise wavenumber ($K_{X,qmn} = 0$, dashed line in Fig. 5). $S_{QQ,qmn}$ exhibits a maximum level at the value of (m, n) corresponding to the smallest values of both the chordwise wavenumber of the turbulence $K_{X,qmn}$ and the aeroacoustic coupling wavenumber κ_{qmn}. This behavior is due to a combination in $S_{QQ,qmn}$ [see Eq. (36)] of the turbulent velocity spectrum Φ_{ww}, which decays rapidly with $K_{X,qmn}$, with the unsteady loading term $|L_{qmn}|^2$, which is maximum for $(K_{X,qmn}, \kappa_{qmn}) \to (0, 0)$, from Eq. (27) and using the flat-plate response functions due to Amiet [8,9].

As shown in Fig. 5b, the radiation term Π_{ml} exhibits sharp cut-off that can be used to limit the maximum value of the m and n summations in Eq. (34). The two limits are specified by $l_{\max}$ and $m_{\max}$, which are the maximum absolute values of l and m above which the acoustic radiation can be neglected. The limit $l_{\max}$ originates from the behavior of the Bessel function of order l in Eq. (35) and is a sharp cut-off condition, whereas the condition $m_{\max}$ originates from the behavior of the Fourier component f_m of the wake profiles of Eq. (6) and is a softer limiting condition.

For Bessel functions $J_l(x)$ of high order l, the value of the argument x_0 at which the Bessel function is no longer negligible can be approximated by $x_0 \approx l$. As suggested in [6] (chapter 1), the cut-on condition $l \le l_{\max}$ can therefore be approximated by $\xi > 1$, where $\xi = x_0/l$. Defining the circumferential phase speed of the azimuthal acoustic mode l at the jth strip as $c_l = \omega \bar{r}_j / l$, the cut-on condition $\xi > 1$ can therefore be satisfied at any θ only if

$$c_l > c_0 \tag{42}$$

Equation (42) confirms the well-known result that only azimuthal modes l whose azimuthal phase speed is supersonic can radiate to the far-field. Based on this argument, the maximum value of l is chosen empirically as

$$l_{\max} = 1.25 \frac{\omega}{c_0} \bar{r}_j \sin\theta + 3 \tag{43}$$

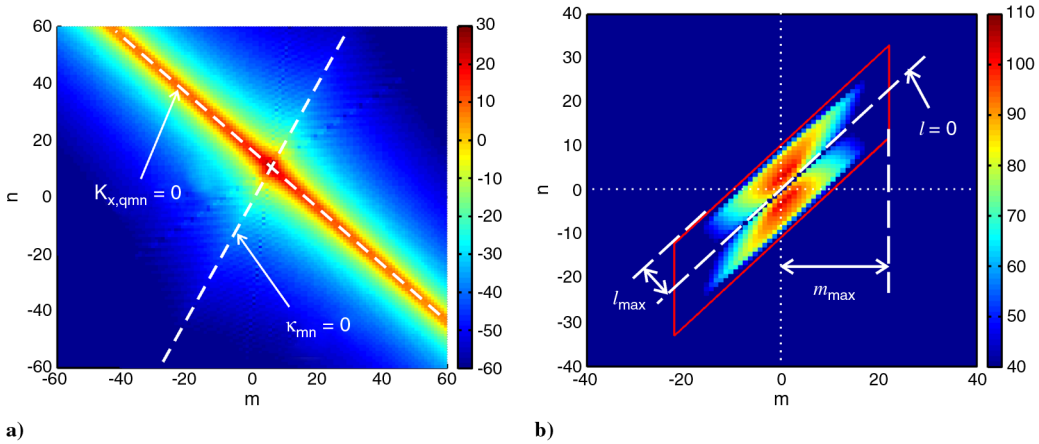

Fig. 5 Variation of a) the source term $S_{QQ,qmn}$, and b) the radiation term Π_{ml} (in dB and for a single strip) with m and n. $f = 8$ kHz, $C_d = 0.1$, $q = 0$, $\theta = 90°$.

to take into account every significant mode l at all frequencies. The Fourier components of the wake profile f_m [Eq. (6)] are defined by a Gaussian function of m with standard deviation $\sigma = \frac{\bar{r}_j\sqrt{2a}}{B_1 b_W}$. The spread of a Gaussian function is proportionally related to the standard deviation σ and, therefore, the maximum value of m that must be included in the modal summation of Eq. (34) must be related to σ and is set to be

$$m_{\max} = 4\sigma = 4\frac{\bar{r}_j\sqrt{2a}}{B_1 b_W} \tag{44}$$

which includes more than 99.99% of the energy distribution over m, according to the 68–95–99.7% rule for Gaussian functions.

Figure 6 shows the variation of $S_{pp,qmn}$ on m and n, for $q = 0$ and $\theta = 90°$, due to a single strip of the rear rotor. The limits $l_{\max}$ and $m_{\max}$ are represented by the parallelogram in Fig. 6. These limits are therefore set conservatively, since a number of nonsignificant indices m and n are included in the summations, especially at low C_d (which yields low b_W) and high frequency, due to the definition of $m_{\max}$. Note also that the computational cost of the model will be low at high blade numbers B_1 and B_2, since $m_{\max} \sim 1/B_1$ and since fewer l modes are needed if B_1 and B_2 are large [see Eq. (17)].

B. Reduction of the Summation over the Turbulence Azimuthal Mode Order q

The identification of clear limits involved in the sum over q are more difficult than for the indices m and n. The limits $l_{\max}$ and $m_{\max}$ have been defined for a single given mode q (see Sec. III.A), and therefore the contribution $S_{pp,q}$ of each mode order q to the radiated broadband noise must be expressed *after* summation over indices m and n, as $S_{pp,q} = \Sigma_m \Sigma_n S_{pp,qmn}$. Contrary to that observed for the reduction of the sums over m and n, the behavior of $S_{pp,q}$ exhibits no

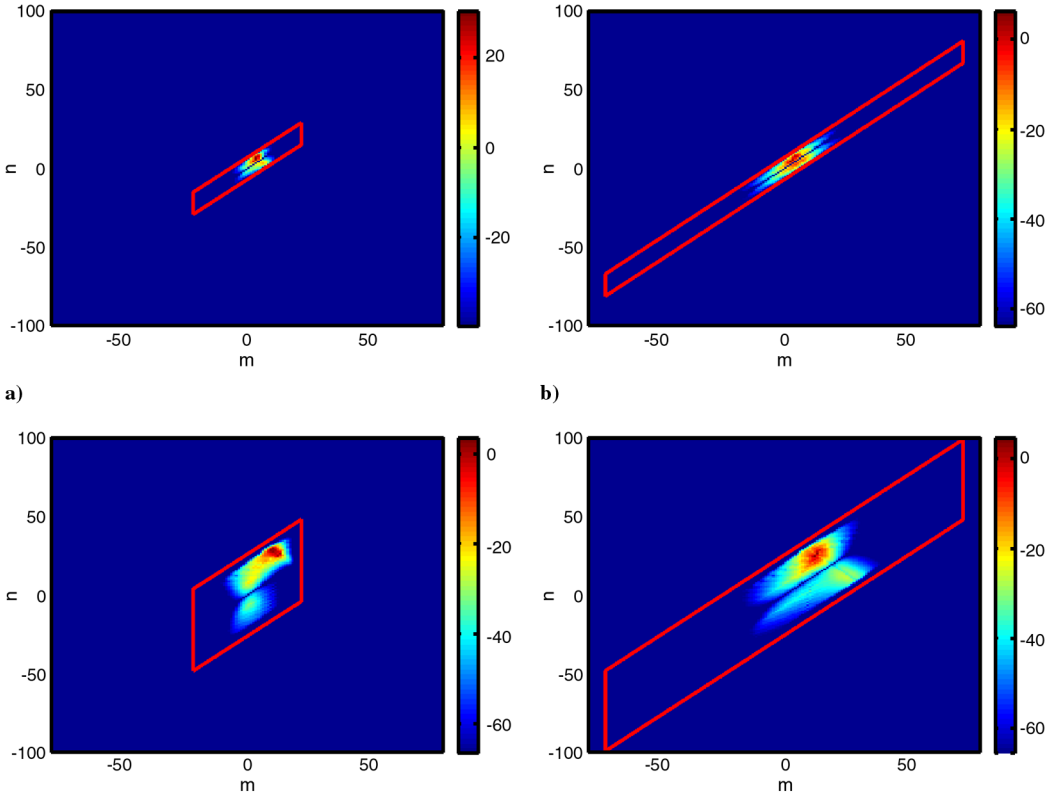

Fig. 6 Variation of $S_{pp,qmn}$ in dB with m and n and validation of the limiting conditions $l_{\max}$ and $m_{\max}$ (red line) for a single strip, $q = 0$, $\theta = 90°$, a) $f = 5$ kHz, $C_d = 0.1$, b) $f = 5$ kHz, $C_d = 0.02$, c) $f = 20$ kHz, $C_d = 0.1$, and d) $f = 20$ kHz, $C_d = 0.02$.

clear cut-off condition. A large number of modes q therefore contributes significantly to the far-field noise. Thus, the sum over q can become an important computational burden, especially at high frequencies where many (m, n) modes are significant. This problem has been partly overcome by using an adaptive integration scheme (adaptive Simpson quadrature) to compute the sum over q at medium and high frequencies. Using this numerical method makes the computation significantly faster, although some care must be taken in its implementation so that all the contributions of the modes q are well captured. $S_{pp,q}$ is generally a smooth well behaved function of q but may exhibit strong oscillatory behavior in the limit of low frequency and high blade number, which yields strong blade-to-blade correlation as explained in Sec. IV.A. In this case, it is our experience that the adaptive integration should be avoided, and the summation over q should therefore be performed exactly over a sufficiently large range of q to ensure convergence.

IV. Parameter Study

A parameter study has been conducted to investigate the sensitivity of the broadband noise predictions to variations in engine parameters such as blade number, rotor–rotor gap and front and rear rotor speed. Blade number effects and rotor–rotor gap effects are investigated for a typical CROR configuration by freezing all other aerodynamic and geometrical parameters. Rotor speed effects are investigated at constant engine power and torque split between the two rotors. The baseline configuration chosen for this parameter study is that of a typical full-scale CROR, at takeoff conditions, and the parameter study is conducted on a single representative spanwise strip of the rotors located at the midspan. The details of the configuration of the CROR and the noise levels are confidential at the time of writing and, therefore, only relative levels of broadband noise are presented in this section, without any loss of generality. The frequency axis is normalized by the blade passing frequency of the rear rotor $f_{\text{ref}} = B_2\Omega_2/2\pi$ for the baseline configuration.

This parameter study, and more specifically the study of rotor–rotor gap effects and rotor speed effects, assumes the validity of the correlation results of Gliebe et al. [10] that were used to model the wake turbulence. Those empirical correlations were established by measuring the velocity fluctuation downstream of a rotor and provide an estimation of the mean and turbulent wake parameters from the drag coefficient C_d of the front blades, the freestream velocity U_{X1} and the helical path length of the wakes. Note that the validity of the turbulence correlations due to Gliebe et al. are confined to the near wake of the rotor, corresponding to approximately $X1/c1 < 100Cd$. These turbulence predictions are therefore likely to be inaccurate at operating conditions where the rotor drag is comparatively low, such as at approach and cruise

A. Blade Number Effects

Figure 7 illustrates the effects of blade number variation on the predicted PWL (in dB) of the broadband noise due to rotor–wake/rotor interaction. Contour plots of PWL are presented for three frequencies and for blade numbers B_1 and B_2 between 6 and 20 (with a step of 2). The variation of the contours of PWL, relative to their value at $B_1 = B_2 = 6$, is shown. The contours of PWL exhibit strong symmetry with respect to B_1 and B_2, with small deviation for large values of B_1 and B_2 in Figs. 7a and 7b.

This blade-to-blade correlation effect for high solidity fans has been first discussed by Mani [25] and Homicz and George [26] (for noise due to turbulence ingestion into a rotor), and occurs when the time scale for eddies to be convected past a given point in the rotor plane is smaller than the blade passage time. In this case, peaks occur at frequencies corresponding to the interaction tones frequency, i.e., at $\omega_{mn} = mB_1\Omega_1 - nB_2\Omega_2$. It appears more clearly as oscillations at low and mid frequencies and high blade number in Fig. 8.

The spectra plotted in Fig. 8a exhibit a clear scaling of the broadband noise due to rotor–wake/rotor interaction with $B_1 \times B_2$. This is demonstrated more clearly in Fig. 8b where the PWL spectra are normalized on $10\log_{10}(B_1B_2)$. The best collapse between the spectra occurs at high frequencies and low blade number, i.e., when blade-to-blade correlation is weak. It should be noted, however, that a more complex sensitivity of PWL with the number of blades B_1 and B_2 would be expected if the engine power was kept constant.

Because the computational cost of the model is small at high blade numbers (see Sec. IV.A), a fast approximate model can be obtained by increasing arbitrarily the number of blades and then normalizing

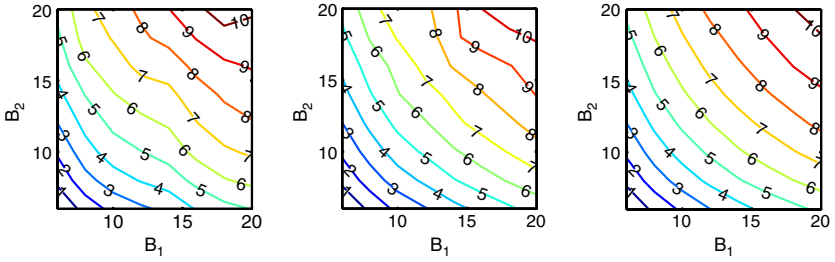

a) $f/f_{ref} = 3.147$ **b)** $f/f_{ref} = 6.294$ **c)** $f/f_{ref} = 62.935$

Fig. 7 Effects of blade number on contour of PWL − PWL$(B_1 = B_2 = 6)$ (in dB).

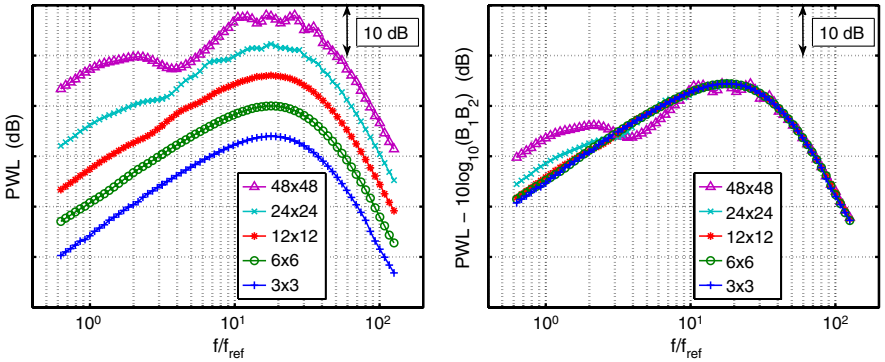

a) **b)**

Fig. 8 Effects of blade number on a) PWL(f), and b) PWL$(f) - 10\log_{10}(B_1B_2)$.

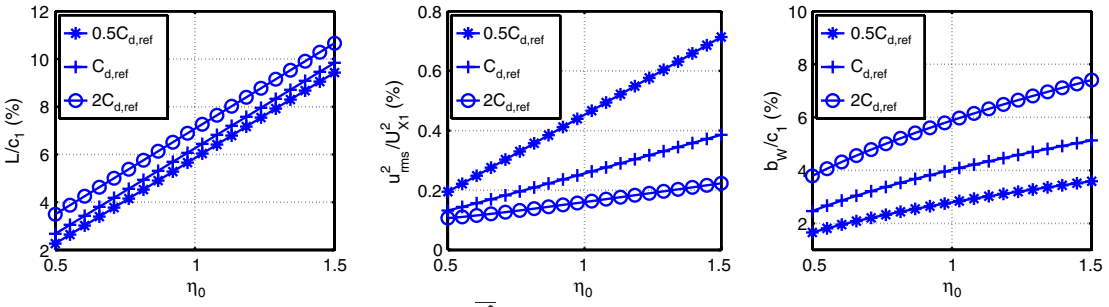

Fig. 9 Variation of the turbulence parameters L and $\overline{u^2}$ and the half-wake width b_W with nondimensional rotor–rotor gap η_0.

the resulting noise levels by $B_1 \times B_2$. The main drawback to this approach is that oscillations such as those of Fig. 8b may appear in the spectrum for configurations where blade-to-blade correlation is strong, even though the main trends in the level and general spectral shape are captured.

B. Rotor–Rotor Gap Effects

In this section the effects of the axial gap between the two rotors on the radiated noise are investigated. A nondimensional gap is defined in this study as $\eta_0 = \eta/\eta_{\text{ref}}$, where η is the actual rotor–rotor gap and η_{ref} is a reference gap corresponding to the one of a typical full-scale CROR. The nondimensional gap η_0 is varied between 0.5 and 1.5 and the impact on wake turbulence is predicted using the near-wake empirical correlations due to Gliebe et al. [10] (as mentioned in Sec. II.B.1). Because wake turbulence is highly sensitive to the drag coefficient C_d of the front rotor airfoils, the effects of rotor–rotor gap are investigated for three typical drag coefficients $C_{d,\text{ref}}$, $2C_{d,\text{ref}}$ and $0.5C_{d,\text{ref}}$, where $C_{d,\text{ref}} = 0.0134$.

The turbulence mean square velocity $\overline{u^2}$, the turbulence integral length scale L and the half-wake width b_W are the parameters most significantly affected by changes in rotor–rotor gap. Figure 9 presents the variation of these parameters, normalized on either c_1 or U^2_{X1}, with nondimensional gap η_0. The parameters L, $\overline{u^2}$ and b_W are found to increase with increasing η. Both L and $\overline{u^2}$ vary nearly linearly with η_0. The rate of growth of L is constant with C_d, while the rate of growth of $\overline{u^2}$ is significantly higher for low C_d.

Figure 10 presents the PWL spectra of broadband noise due to rotor–wake/rotor interaction for $\eta_0 = 0.5$ to 1.5 (with a step of 0.1) for the three values of C_d under investigation. The effect of rotor–rotor gap on broadband noise emissions is strong for the cases considered, since the differences between the PWL for the two extreme gaps considered can reach up to 35 dB. Increasing the rotor–rotor gap yields a strong increase in the spectrum level at low frequencies, whereas a much smaller increase is observed at high frequencies. These effects are consistent with the asymptotic scaling laws of Eq. (39) with the input values of L, $\overline{u^2}$, and b_W shown in Fig. 9, as explained below.

Figure 11 presents plots of normalized PWL as a function of η_0 for 75 frequency points corresponding to the frequencies shown in Fig. 10. The spectra have been normalized by their value at $\eta_0 = 0.5$ at each frequency, such that $\Delta\text{PWL}(\eta_0) = \text{PWL}(\eta_0) - \text{PWL}(0.5)$. The effect of rotor–rotor gap on the broadband noise due to rotor–wake/rotor interaction is found to be strong for the typical CROR configuration under investigation. Reducing the rotor–rotor gap tends to reduce significantly the broadband noise due to rotor–wake/rotor interaction, especially in the low and medium frequency ranges. Moreover, excellent agreement is observed in Fig. 11 between the predicted PWL and the theoretical high- and low-frequency scaling laws given in Eq. (39), denoted by the dashed curves. Note that the

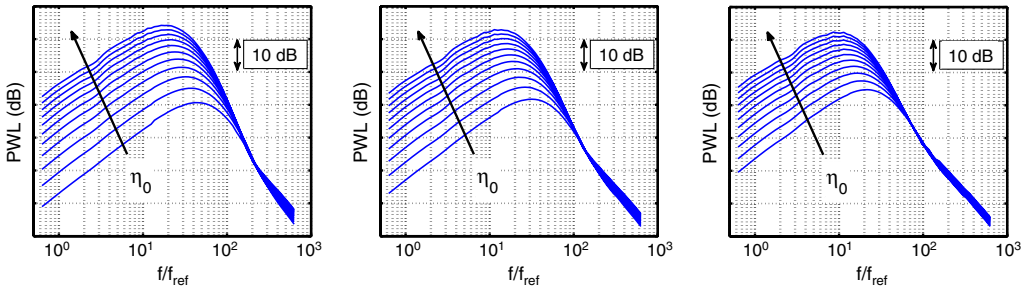

a) $C_d = 0.5C_{d,ref}$ **b) $C_d = C_{d,ref}$** **c) $C_d = 2C_{d,ref}$**

Fig. 10 Effect of rotor–rotor gap on PWL spectra, for $\eta_0 = 0.5$ to 1.5.

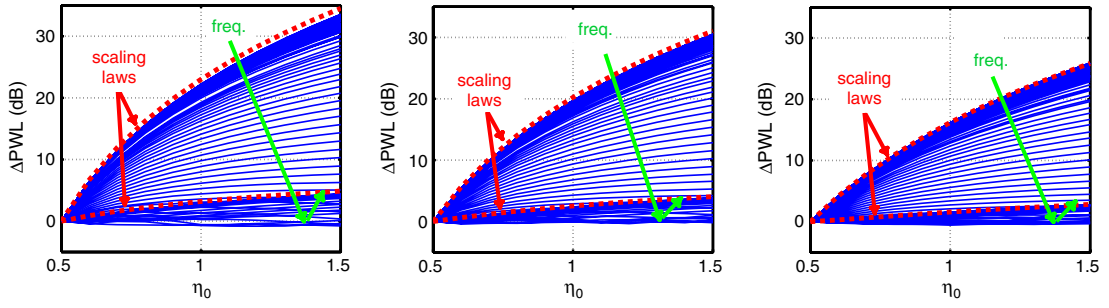

a) $C_d = 0.5C_{d,ref}$ **b) $C_d = C_{d,ref}$** **c) $C_d = 2C_{d,ref}$**

Fig. 11 ΔPWL as a function of η_0 for all frequency points.

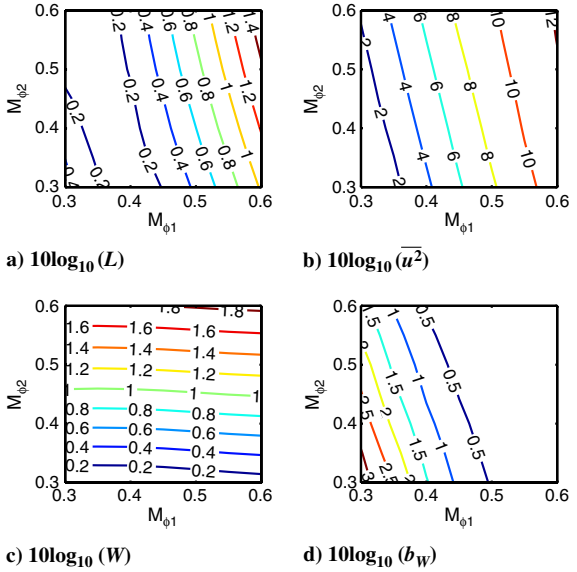

Fig. 12 Variation (in dB) of L, $\overline{u^2}$, W, and b_W, relative to their minimum value, with $M_{\phi 1}$ and $M_{\phi 2}$, at constant engine power and torque split.

high-frequency asymptote is not reached monotonically but overshoots before reaching the asymptotic value.

The results presented in this section show that increasing the axial gap between the rotors yields an increase in broadband noise emissions. However, increasing the rotor–rotor gap in CRORs would also decrease the tonal noise emissions due to both the rotor–wake/rotor interaction and the potential field interaction between the two rotors. It should therefore be possible to define an optimized gap which would balance the contributions of the tonal and the broadband noise.

C. Rotor Speed Effects at Constant Power and Torque Split

In this section the effects of front and rear rotor speed on the broadband noise due to rotor–wake/rotor interaction are investigated. This study is performed while keeping constant the power of the engine and the torque split between the rotors, to investigate the variation of the noise for realistic engine configurations. The desired torque split, power and rotor speeds are input to a thermodynamic design model, which gives as output the flow velocities and the stagger angles of both rotors. As previously, we consider a single strip located at the midspan of both rotors. The rotational Mach numbers of each rotor are varied from $M_{\phi 1,2} = U_{\phi 1,2}/c_0 = 0.3$ to 0.6.

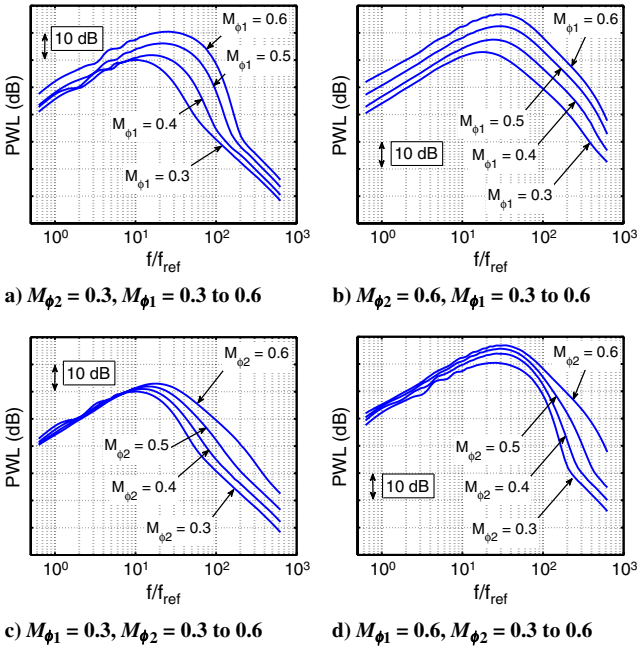

Fig. 14 Effects of rotor speed on PWL spectra.

The variation with $M_{\phi 1}$ and $M_{\phi 2}$ of the input parameters to the current model is generally complex and is worth some attention. Because of the constraint of constant power and torque split, many parameters will vary at the same time in the noise model. Figure 12 shows the variation with $M_{\phi 1}$ and $M_{\phi 2}$ of the parameters appearing in the scaling laws of Eq. (39) (normalized by their smallest value) for the configuration considered. As shown in Fig. 12, the turbulent wake parameters $\overline{u^2}$, L and b_W are clearly more sensitive to $M_{\phi 1}$ than to $M_{\phi 2}$. This is consistent with the fact the stagger angles of both rotors are adjusted to maintain constant power and torque split. The variation of $M_{\phi 1}$ therefore modifies the length of the wake helical path, to which the steady and turbulent parameters are intimately linked. The fact that the stagger angles are adjusted also explains why the increase in the flow velocity W is relatively small between the low-speed case ($M_{\phi 1} = M_{\phi 2} = 0.3$) and the high-speed case ($M_{\phi 1} = M_{\phi 2} = 0.6$).

Contour plots of the variation of PWL with $M_{\phi 1}$ and $M_{\phi 2}$, at several frequencies, are shown in Fig. 13. The variation of rotor speed, at constant power and torque split, appears to have a strong effect on broadband noise due to rotor–wake/rotor interaction. For the CROR

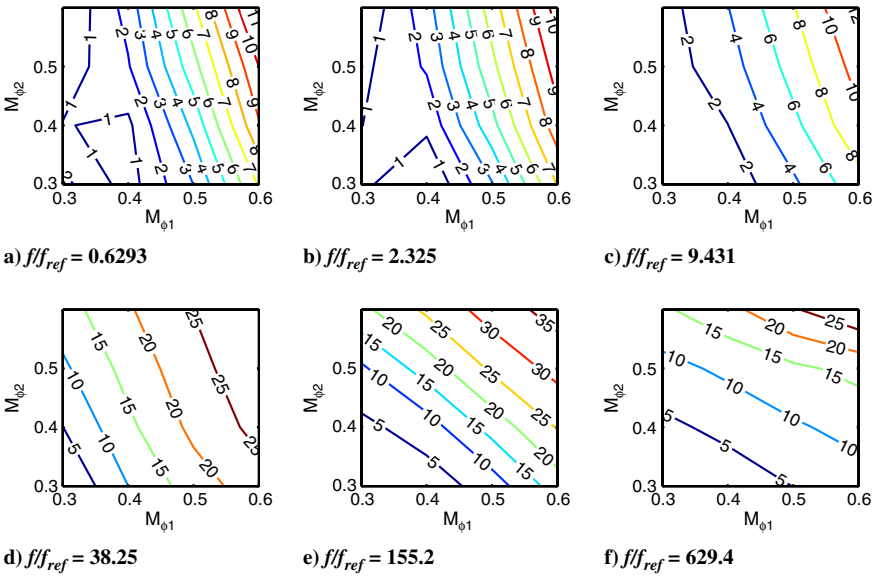

Fig. 13 Contours plots of PWL with $M_{\phi 1}$ and $M_{\phi 2}$ at several frequencies. Levels are relative to the minimum value of each contour plot.

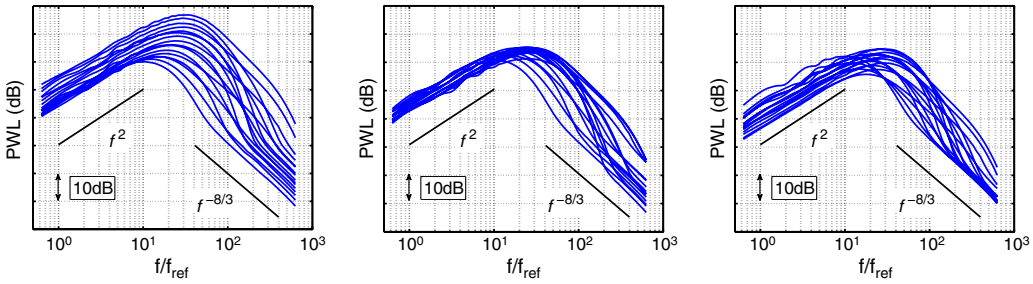

a) No normalization b) Low frequency scaling law c) High frequency scaling law

Fig. 15 Effects of $M_{\phi 1}$ and $M_{\phi 2}$ on PWL spectra without a) and with normalization by low- b) or high-frequency scaling laws.

configuration considered, the increase in broadband noise level predicted from the low- to the high-speed case can reach up to 35 dB at certain frequencies. The shape of the noise contours can be understood by comparing the variation of the input parameters, shown in Fig. 12, and the low and high frequencies scaling laws of Eq. (39). The overall variation of the PWL contours at low frequency (Fig. 13a) is similar to the contour plot for the variation of L (Fig. 12a). This suggests that effects of L on PWL are strong at low frequencies. Moreover, in the low and medium frequency range, the PWL seems to be more sensitive to $M_{\phi 1}$ than to $M_{\phi 2}$. However, this trend is observed to reverse at high frequencies. This is in agreement with Eq. (39), which states that effects of L should dominate at low frequency and effects of W should dominate at high frequency. A more detailed validation of the scaling laws of Eq. (39) is now conducted by analyzing the PWL spectra.

Figure 14 presents the PWL spectra obtained while fixing the speed of one of the two rotors (to either $M_{\phi 1,2} = 0.3$ or 0.6) while varying the speed of the other rotor. The general shape of the spectra can be divided into three frequency bands: a low-frequency asymptotic region, where "humps" can appear if blade-to-blade correlation is significant, a high-frequency asymptotic region, and a mid frequency region that includes the spectrum peak followed by a strong decay. This mid frequency decay is due to the wake profile term f_m (Eq. (6)) which is a Gaussian function of the index m. The strength of this decay is linked to the value of the half-wake width b_W. Note that, for the configurations considered, the high-frequency asymptotic range is usually reached at very high frequencies, often above 20 kHz (see, for instance, the $M_{\phi 1,2} = 0.6$ configurations).

The spectra for all the rotor speeds tested are plotted together in Fig. 15 with and without normalization by the scaling laws established in Eq. (39). The asymptotic behavior of the PWL with frequency, in the low and high-frequency limit, is verified. The collapse of the spectra observed is reasonable at high frequency (Fig. 15c), for the spectra which have reached their asymptotic region, but is only reasonably good at low frequency (within 5 dB in Fig. 15b). This has been attributed to the presence of blade-to-blade correlation (see Sec. IV.A), leading to low-frequency humps in the spectra that cannot be captured by the scaling laws.

V. Conclusions

A semi-analytical model for the far-field broadband noise due to rotor–wake/rotor interaction in CRORs has been presented in detail. The model combines a semi-analytical model developed for tone prediction with classical isolated flat-plate theory to model the response function of the rear blade row due to the excitation by turbulent wakes. Wake turbulence is assumed to be homogeneous and isotropic, modulated by a train of wake profiles, and the wake parameters are deduced from near-wake empirical correlations. Insight into the modal behavior of the model has been presented.

A parameter study has been conducted to investigate the effects of blade number, rotor–rotor gap and rotor speed on the PWL of rotor–wake/rotor interaction broadband noise in CRORs. For the realistic CROR configuration tested, it has been observed that:

1) Broadband noise levels scale well with $B_1 \times B_2$, provided that blade-to-blade interaction is not significant (i.e., rear blades are well separated and eddies are small).

2) Reducing the axial gap between the rotors yields a significant reduction of the broadband noise predictions. This comes from the fact that the integral lengthscale of the turbulence decreases significantly when the axial gap decreases. The resulting noise reduction is most important at low and medium frequencies, where the broadband noise is most sensitive to the integral lengthscale.

3) For constant engine power and torque split, broadband noise emissions are predicted to increase with both front and rear rotor speed, but are more sensitive to changes in the front rotor speed at low and mid frequencies.

Moreover, scaling laws were established to described the asymptotic behavior of the broadband noise emission in the low and high-frequency limits. These were validated using the results of the parameter study on the effects of rotor–rotor gap and rotor speed.

Appendix A: Sound Power Radiation with Flow Effects Included

The expressions for the far-field pressure derived in Sec. II.B assume that the medium of acoustic radiation is at rest. This assumption is generally reasonable at low subsonic flight speeds, but the effects of the uniform mean flow, of Mach number M_x, must be included in the final expression for PWL. The pressure spectrum with mean flow $\breve{p}$ may be deduced from the no-flow solution $\hat{p}$ of Eq. (26) by Lorentz transformation (note that the convention $\hat{(.)}$ denoting a frequency domain quantity has been dropped for the sake of clarity). According to the work of Chapman [27], the results of this transform can be generalized in a simple form as

$$\breve{p}(r_0, \theta, \psi_0, \omega) = p(\breve{r}_0, \breve{\theta}, \psi_0, \omega) e^{ik_0 r_0 M_x \cos\theta/\beta^2} \tag{A1}$$

where $\beta_x = \sqrt{1 - M_x^2}$ and the equivalent flow corrected radiation distance $\breve{r}_0$ and angle $\breve{\theta}$ may be obtained from their no-flow values as

$$\breve{r}_0 = \frac{r_0}{\beta_x^2}\sqrt{1 - M_x^2 \sin^2\theta}, \qquad \cos\breve{\theta} = \frac{\cos\theta}{\sqrt{1 - M_x^2\sin^2\theta}} \quad \text{and}$$
$$\sin\breve{\theta} = \frac{\beta_x \sin\theta}{\sqrt{1 - M_x^2\sin^2\theta}} \tag{A2}$$

The notation $\breve{(.)}$ is used to represent a quantity expressed following Chapman's similarity rule. Substituting Eq. (26) into Eq. (A1) allows the effects of a uniform mean flow to be included into the expression for the modal pressure spectrum radiated to the far field

$$\breve{p}_{qmn}(r_0, \theta, \psi_0, \omega) = \frac{-i}{8\pi^2}\frac{\rho_0 c_2 B_2}{2\breve{r}_0} e^{-i[k_0 r_0 S(\theta, M_x) - l(\frac{\pi}{2} + \psi_0)]}$$
$$\times \int_{R_{h2}}^{R_{t2}} f_m(r)\left(\frac{l}{r} + \frac{\omega}{c_0}\cos\breve{\theta}\tan\alpha_2\right)\frac{J_l(\frac{\omega}{c_0} r \sin\breve{\theta})}{r}$$
$$\times \int_{-\infty}^{\infty} \mathcal{W}(k_r, K_{X,qmn}, K_{Y,qmn}) L_{qmn}(k_r, K_{X,qmn}, \breve{\kappa}_{qmn}) e^{-ik_r r}\, \mathrm{d}k_r\, \mathrm{d}r \tag{A3}$$

where the aeroacoustic coupling wavenumber $\breve{\kappa}_{qmn}$ have been transformed accordingly from Eqs. (21) and (28), and where $S(\theta, M_x) = (\sqrt{1 - M_x^2\sin^2\theta} - M_x\cos\theta)/\beta_x^2$.

From the classical work of Morfey [28], the expression of the acoustic intensity towards the observer in an isentropic and potential flow can be expressed as

$$I_R(r_0,\theta,\psi_0,\omega)=\frac{1}{2}Re\left\{\breve{p}\breve{u}_R^*+\frac{M_x\cos\theta}{\rho_0 c_0}|\breve{p}|^2 + M_x^2\cos\theta\breve{p}\breve{u}_x^*+M_x\rho_0 c_0\breve{u}_R\breve{u}_x^*\right\} \tag{A4}$$

where $\breve{u}_R$ and $\breve{u}_x$ are the components of the acoustic velocity fluctuation in the radial and axial direction, respectively.

Using the momentum equation, direct relations can be established between $\breve{u}_R$, $\breve{u}_x$, and $\breve{p}$ using the velocity potential and neglecting the terms of order $\mathcal{O}(1/r_0)$ as

$$\breve{u}_R(r_0,\theta,\psi_0,\omega)=\sqrt{1-M_x^2\sin^2\theta}\frac{\breve{p}(r_0,\theta,\psi_0,\omega)}{\rho_0 c_0} \tag{A5}$$

$$\breve{u}_x(r_0,\theta,\psi_0,\omega)=(\sqrt{1-M_x^2\sin^2\theta}\cos\theta - M_x\sin^2\theta)\frac{\breve{p}(r_0,\theta,\psi_0,\omega)}{\rho_0 c_0} \tag{A6}$$

The expression of the radial time averaged intensity is then obtained by substituting Eqs. (A5) and (A6) into Eq. (A4) to give

$$I_R(r_0,\theta,\psi_0,\omega)=\frac{|\breve{p}(r_0,\theta,\psi_0,\omega)|^2}{2\rho_0 c_0}F(\theta,M_x) \tag{A7}$$

where $F(\theta,M_x)=\sqrt{1-M_x^2\sin^2\theta}/S^2(\theta,M_x)$.

The final expression for PWL in decibels can then be obtained by integrating the expected value of Eq. (A7) over a sphere (assuming axisymmetry of the directivity of axis $\theta=0$), which is shown in Eqs. (40) and (41). Note that an approach similar to that presented in this appendix has been used by Sinayoko et al. [29] to compute the sound power radiated from a semi-infinite duct with uniform flow.

Acknowledgments

This work has been funded by the FP7 European project Validation of Radical Engine Architecture Systems (DREAM) and Rolls-Royce plc. The authors would like to thank A. B. Parry and S. Baralon from Rolls-Royce plc. for their support and advice.

References

[1] Hanson, D. B., "Noise of Counter-Rotation Propellers," *Journal of Aircraft*, Vol. 22, No. 7, 1985, pp. 609–617. doi:10.2514/3.45173

[2] Parry, A. B., "Theoretical Prediction of Counter-Rotating Propeller Noise," Ph.D. Thesis, Univ. of Leeds, 1988.

[3] Parry, A. B., "Modular Prediction Scheme for Blade Row Interaction Noise," *Journal of Propulsion and Power*, Vol. 13, No. 3, 1997, pp. 334–341. doi:10.2514/2.5186

[4] Parry, A. B., and Crighton, D. G., "Prediction of Counter-Rotation Propeller Noise," *12th AIAA Aeroacoustics Conference*, AIAA 1989-1411, 1989.

[5] Whitfield, C. E., Gliebe, P. R., Mani, R., and Mungur, P., "High Speed Turboprop Aeroacoustic Study (Counter-Rotation) Vol. 1: Model Development," NASA Tech. Rept. 185241, 1990.

[6] Hubbard, H. H., "Aeroacoustics of Flight Vehicles, Theory and Practice Volume 1. Noise Sources," Vol. 1, NASA Reference Publication, 1991.

[7] Amiet, R. K., "Acoustic Radiation from an Airfoil in a Turbulent Stream," *Journal of Sound and Vibration*, Vol. 41, No. 4, 1975, pp. 407–420. doi:10.1016/S0022-460X(75)80105-2

[8] Amiet, R. K., "Compressibility Effects in Unsteady Thin-Airfoil Theory," *AIAA Journal*, Vol. 12, No. 2, 1974, pp. 252–255. doi:10.2514/3.49212

[9] Amiet, R. K., "High Frequency Thin-Airfoil Theory for Subsonic Flow," *AIAA Journal*, Vol. 14, No. 8, 1976, pp. 1076–1082. doi:10.2514/3.7187

[10] Gliebe, P., Mani, R., Shin, H., Mitchell, B., and Ashford, G., "Aeroacoustic Prediction Codes," NASA, Tech. Rept. 210244, 2000.

[11] Blandeau, V. P., Joseph, P. F., and Tester, B. J., "Broadband Noise Prediction from Rotor-Wake Interaction in Contra-Rotating Propfans," *15th AIAA/CEAS Aeroacoustics Conference*, AIAA, 2009-3137, 2009.

[12] Casper, J., and Farassat, F., "A New Time Domain Formulation for Broadband Noise Predictions," *International Journal of Aeroacoustics*, Vol. 1, No. 3, 2002, pp. 207–240. doi:10.1260/147547202320962574

[13] Farassat, F., Dunn, M. H., Tinetti, A. F., and Nark, D. M., "Open Rotor Noise Prediction Methods at NASA Langley: A Technology Review," *15th AIAA/CEAS Aeroacoustics Conference*, AIAA 2009-3133, 2009.

[14] Devenport, W. J., Staubs, J. K., and Glegg, S. A. L., "Sound Radiation from Real Airfoils in Turbulence," *Journal of Sound and Vibration*, Vol. 329, No. 17, 2010, pp. 3470–3483. doi:10.1016/j.jsv.2010.02.022

[15] Jurdic, V., Moreau, A., Joseph, P. F., Enghardt, L., and Coupland, J., "A Comparison Between Measured and Predicted Fan Broadband Noise Due to Rotor-Stator Interaction," *13th AIAA/CEAS Aeroacoustics Conference*, AIAA, 2007-3692, 2007.

[16] Jurdic, V., Joseph, P., and Antoni, J., "Investigation of Rotor Wake Turbulence Through Cyclostationary Spectral Analysis," *AIAA Journal*, Vol. 47, No. 9, 2009, pp. 2022–2030. doi:10.2514/1.36728

[17] Wygnanski, I., Champagne, F., and Marasli, B., "On the Large-Scale Structures in Two-Dimensional, Small-Deficit, Turbulent Wakes," *Journal of Fluid Mechanics*, Vol. 168, 1986, pp. 31–71.

[18] Ventres, C. S., Theobald, M. A., and Mark, W. D., "Turbofan Noise Generation. Volume 1: Analysis," NASA, Tech. Rept. 167951, 1982.

[19] Lloyd, A. E. D. and Peake, N., "Rotor–Stator Broadband Noise Prediction," *14th AIAA/CEAS Aeroacoustics Conference*, AIAA, 2008-2840, 2008.

[20] Nallasamy, M., and Envia, E., "Computation of Rotor Wake Turbulence Noise," *Journal of Sound and Vibration*, Vol. 282, Nos. 3–5, 2005, pp. 649–678.

[21] Amiet, R. K., "Noise Produced by Turbulent Flow into Rotor: Theory Manual for Noise Calculation," NASA Tech. Rept. 181788, 1989.

[22] Hanson, D. B., and Horan, K., "Turbulence/Cascade Interaction: Spectra of Inflow, Cascade Response, and Noise," *4th AIAA/CEAS Aeroacoustic Conference*, AIAA 1998-2319, June 1998.

[23] Ffowcs-Williams, J. E., and Hawkings, D. L., "Sound Generation by Turbulence and Surfaces in Arbitrary Motion," *Philosophical Transactions of the Royal Society of London, Series A: Mathematical and Physical Sciences*, Vol. 264, No. 1151, 1969, pp. 321–342.

[24] Posson, H., Moreau, S., and Roger, M., "Fan-OGV Broadband Noise Prediction Using a Cascade Response," *15th AIAA/CEAS Aeroacoustics Conference*, AIAA 2009-3150, 2009.

[25] Mani, R., "Noise Due to Interaction of Inlet Turbulence with Isolated Stators and Rotors, *Journal of Sound and Vibration*, Vol. 17, No. 2, 1971, pp. 251–260.

[26] Homicz, G., and George, A., "Broadband and Discrete Frequency Radiation from Subsonic Rotors," *Journal of Sound and Vibration*, Vol. 36, No. 2, 1974, pp. 151–177. doi:10.1016/S0022-460X(74)80292-0

[27] Chapman, C., "Similarity Variables for Sound Radiation in a Uniform Flow," *Journal of Sound and Vibration*, Vol. 233, No. 1, 2000, pp. 157–164.

[28] Morfey, C. L., "Acoustic Energy in Non-Uniform Flows," *Journal of Sound and Vibration*, Vol. 14, No. 2, 1971, pp. 159–170.

[29] Sinayoko, S., Joseph, P., and McAlpine, A., "Multimode Radiation from an Unflanged, Semi-Infinite Circular Duct with Uniform Flow," *Journal of the Acoustical Society of America*, Vol. 127, No. 4, 2010, pp. 2159–2168. doi:10.1121/1.3327814

C. Bailly
Associate Editor